Quasi-periodic oscillations and particle motion around charged black hole surrounded by a cloud of strings and quintessence field in Rastall gravity

Physica Scripta

PAPER

Quasi-periodic oscillations and particle motion around charged black hole surrounded by a cloud of strings and quintessence field in Rastall gravity

Asifa Ashraf[1], **Allah Ditta**[2], **Değer Sofuoğlu**[3], **Wen-Xiu Ma**[1,4,5,6,*], **Faisal Javed**[7], **Farruh Atamurotov**[8,9,10] **and Asif Mahmood**[11]

[1] School of Mathematical Sciences, Zhejiang Normal University, Jinhua, Zhejiang 321004, People's Republic of China
[2] Department of Mathematics, Shanghai University and Newtouch Center for Mathematics of Shanghai University, Shanghai, 200444, People's Republic of China
[3] Department of Physics, Istanbul University, 34134, Vezneciler, Fatih, Istanbul, Turkey
[4] Department of Mathematics, King Abdulaziz University, Jeddah 21589, Saudi Arabia
[5] Department of Mathematics and Statistics, University of South Florida, Tampa, FL 33620-5700, United States of America
[6] School of Mathematical and Statistical Sciences, North-West University, Mafikeng Campus, Private Bag X2046, Mmabatho 2735, South Africa
[7] Department of Physics, Zhejiang Normal University, Jinhua 321004, People's Republic of China
[8] New Uzbekistan University, Movarounnahr street 1, Tashkent 100000, Uzbekistan
[9] University of Tashkent for Applied Sciences, Str. Gavhar 1, Tashkent 100149, Uzbekistan
[10] Institute of Theoretical Physics, National University of Uzbekistan, Tashkent 100174, Uzbekistan
[11] College of Engineering, Chemical Engineering Department, King Saud University Riyadh, Saudi Arabia
[*] Author to whom any correspondence should be addressed.

E-mail: asifamustafa3828@gmail.com, mradshahid01@gmail.com, degers@istanbul.edu.tr, mawx@cas.usf.edu, faisaljaved.math@gmail.com, atamurotov@yahoo.com **and** ahayat@ksu.edu.sa

Keywords: particle motion, Rastall gravity, quasi-periodic oscillations

OPEN ACCESS

RECEIVED
24 February 2024

REVISED
21 March 2024

ACCEPTED FOR PUBLICATION
12 April 2024

PUBLISHED
3 May 2024

Abstract

This work mainly focuses on unveiling the particle dynamics features of black holes. For this objective, we utilize the charged black hole geometry consisting of the cloud strings and quintessence under the ansatz of Rastall gravity. We have calculated and analyzed the effective potential, angular momentum, particle energy, horizon radius, inner stable circular orbit, photon sphere radius, quasi-periodic oscillations, and effective force to reveal the dynamical features. We in detail discussed the effects of charge in black hole, Rastall parameter, strings of cloud parameter, and quintessential parameter on the calculated results. To ensure the scenario of accelerated expansion, ω_q lies in the range $-1 < \omega_q < -1/3$. From this specific range, we choose $\omega_q = -2/3$.

1. Introduction

The widely accepted general relativity (GR) theory is considered to be an interesting and elegant theory and has been tested extensively with consistent results in most cases [1–3]. The recent discovery of gravitational waves (GWs) by the variability of solar irradiance and gravity oscillations (Virgo) and laser interferometer gravitational wave observatory (LIGO) in 2015, through the merger of black holes (BHs), provided strong evidence in support of GR [4]. Since then, numerous GW events have been detected leading to a new realm of research in GW astronomy and a testing ground for various gravity theories including GR under extreme conditions [5–11]. GR has significantly enhanced our understanding of the Universe, but still has limitations such as being unable to explain the cosmic accelerated expansion, encountering infinities in the theory at a highly relativistic regime and not providing predictions for the dark components of the Universe [12–16]. In response to these limitations, there are ongoing attempts to modify the theory.

The ΛCDM (Λ cold dark matter) model is the most favored modification of GR that incorporates the dark components of the observable universe as supplementary fields, and is consistent with current cosmological observations [17, 18]. This simple model assumes a spatially flat, homogeneous, and isotropic universe filled

with a constant energy density fluid called the cosmological constant Λ [18]. However, the ΛCDM model has limitations, such as the inability to justify the existence of Λ or explain its small value, which creates a fine-tuning problem [18]. To address these issues, modified theories of gravity (MTGs) have been proposed, which can predict observational data without invoking the dark components of the Universe [19, 20]. MTGs have enabled the study of GWs, and the emergence of new properties of GWs, such as the presence of a scalar polarization mode in the metric formalism of $f(R)$ theory [19, 21]. This has stimulated research in the field, leading to predictions of deviations from GR in applications to BHs and stellar dynamics. Recent observations have constrained the extra polarization modes of GWs, including the mass of the graviton [22, 23]. Recent observations have constrained the presence of extra polarization modes in GWs and have established a bound on the mass of the quanta of massive mode, graviton, as $m_g \leqslant 7.7 \times 10^{-23} eV/c^2$ [23].

Rastall [24] proposed a modification to GR in 1972 where he suggested that in curved spacetime or in the presence of massive objects, the covariant derivative of the energy-momentum tensor should not be zero, but instead only zero in flat spacetime. This resulted in the Rastall gravity model, which has received attention for its unique characteristic of violating energy conservation in the presence of background curvature. The Rastall theory suggests that the covariant derivative of the energy-momentum tensor should be equal to the divergence of the Ricci scalar or curvature scalar R, while maintaining the Bianchi identity of the vanishing divergence of the Einstein tensor [25]. Although the violation of the conservation, principle is exclusive to Rastall theory, other theories like $f(R, T)$ theory and $f(R, L_M)$ theory exhibit the same feature inherently [25, 26]. Rastall gravity causes significant deviations from GR, particularly near high curvature regimes such as regions surrounding BHs and neutron stars. Despite being equivalent to GR in some aspects, the Rastall theory shows significant deviations from GR in the presence of non-zero curvature or dark energy fields [27]. Recently, the Rastall theory has found important applications in the literature, including rotating and non-rotating BH solutions [28–30], the gravitational collapse of a homogeneous perfect fluid [31], and the the phenomenon of particle creation in Rastall cosmology [32]. Recently, Javed and his collaborators [33] investigated the wormhole solution and thermodynamics of BHs solutions in different modified theories of gravity.

Notably, all vacuum solutions of GR and the modified Rastall theory (RT) are shared. Nevertheless, the non-vacuum solutions exhibit notable distinctions from those in GR when the Radstall parameter λ is taken into account. Researchers became more interested in RT as a result, as seen by their varied views about the novelty and accuracy of RT. Despite the growing interest among researchers to investigate the intriguing and enigmatic characteristics of the RT, Visser [34] has argued that the RT is merely GR's counterpart. Darabi *et al* [35, 36] dissented, contending that Visser's assertion was untrue and that these ideas are different. Visser contended that Rastall's energy-momentum-tensor (EMT) idea was faulty and that it was merely a rearrangement. On the other hand, Darabi *et al* contended that Rastall's concept of EMT was in line with the accepted definition of EMT. Using the same technique as Visser [34], they provided a convincing example of the $f(R)$ theory of gravity to support their claim, proving that it is not the same as general relativity. Since GR can be recovered for a given value of λ, or the Rastall parameter, the RT is essentially a modified version of GR. It is important to note that the recent work by Hansraj *et al* [37] provided support for the extensive analysis conducted by Darabi *et al* [35, 36]. Some interesting works in other versions of RT are present [38–40].

In the current field of study, BHs are regarded as one of the most characteristic features of powerful gravitational fields. The strong gravitational force of a BH means that nothing (particles or radiation) from its event horizon, yet it however swallows everything in its vicinity. In addition to defining some impressive classical discoveries, these thermodynamic entities also provide a clearer picture of the quantum gravitational properties they exhibit. Well-known BH configurations exhibit curvature singularity outside their event horizons; these include the Schwarzschild, Reissner-Nordstr öm (RN), Kerr, and Kerr-Newmann configurations. Alternatively, it is necessary to verify the accuracy of solutions of the GR or alternative theories of gravity by conducting tests based on various astrophysical phenomena. X-ray data obtained from astrophysical compact objects can be a valuable tool for testing specific theories and corresponding solutions [41–44]. Another approach is to use test particles' movements around BHs to model certain processes related to the accretion disc [45, 46]. The electromagnetic field surrounding BHs plays a crucial role in determining the movements of charged particles and other relevant astrophysical processes in the vicinity of the BH. Electromagnetic fields and adjustments made to gravity's laws have been widely examined in references [47–51], with many research projects focused on exploring how the electromagnetic field and parameters of compact objects influence the dynamics of charged particles (for example, [52–60]. Furthermore, the study of electromagnetic fields' effects on particle motion in the background of non-zero magnetic dipoles in the compact object's gravitational field has been examined in the following references [61–66]. In recent studies, authors [67–73] have discussed particle dynamics in BH. Authors [74–76] have discussed the BH geometries haven the quintessence field and clouds of strings.

Here, we plan to explore the charged particle dynamics surrounded by the cloud of strings and quintessence filed in the Rastall gravity black hole vicinity. In section 2 we briefly describe the charged black hole spacetime in Rastall gravity. In section 3 we study the motion of charged massive particles. In section 4, we discuss massless

particle dynamics. Section 5 focuses on the collision of test particles around the magnetized black hole. Section 6 comprehends the discussion about the effective force. Section 7 is devoted to the concluding remarks of the obtained results. Throughout the manuscript, we use a system of units in which $G = c = 1$.

2. Charged black hole solutions surrounded by a cloud of strings and quintessence field (CBHSCSQ) in rastall gravity

According to the study presented in reference [77], Rastall gravity is a modified version of General Relativity that alters the conventional covariant conservation condition of $T^{\mu\nu}_{;\nu} = 0$ to a new form:

$$\nabla_\nu T^{\mu\nu} = \lambda \nabla^\mu R, \tag{1}$$

where λ is a representation of the Rastall parameter. The modified energy-momentum conservation condition in Rastall gravity alters the general conservation of energy and momentum in the presence of non-zero curvature. However, when the curvature approaches zero, meaning no matter-energy contents are present, the theory approximates to the General Relativity (GR). The resulting field equations in Rastall gravity are provided in the following form [24, 77]:

$$R_{\mu\nu} - \frac{1}{2}(1 - 2\zeta) g_{\mu V} R = \kappa T_{\mu\nu}. \tag{2}$$

Considering the trace of the above-given equation, one can obtain

$$R = \frac{\kappa}{(4\zeta - 1)} T, \quad \zeta \neq 1 \Big/ 4, \tag{3}$$

in this scenario, we consider $\zeta = \kappa\lambda$, and in the next discussion, we shall represent the Rastall parameter by ζ. To serve the purpose of obtaining the black hole solutions in the given framework, we use the following ansatz:

$$ds^2 = f(r) dt^2 - \frac{dr^2}{f(r)} - r^2 d\Omega^2, \tag{4}$$

here, $f(r)$ describe the Schwarzschild metric function and $d\Omega^2 = d\theta^2 + \sin^2\theta d\phi^2$ for spherically symmetric general spacetime. The Rastall tensor is defined as $\mathcal{S}\mu\nu = \mathcal{G}\mu\nu + \zeta g_{\mu\nu} R$, where $\mathcal{G}_{\mu\nu}$ represents the Einstein tensor. The components of the Rastall tensor are as follows:

$$\begin{aligned}
\mathcal{S}^0_0 &= \mathcal{G}^0_0 + \zeta R = \tfrac{1}{f(r)}\mathcal{G}_{00} + \zeta R = -r^{-2}\{f'(r)r - 1 + f(r)\} + \zeta R,\\
\mathcal{S}_{11} &= \mathcal{G}^1{}_1 + \zeta R = -f(r)\mathcal{G}_{11} + \zeta R = -r^{-2}\{f'(r)r - 1 + f(r)\} + \zeta R,\\
\mathcal{S}^2_2 &= \mathcal{G}^2{}_2 + \zeta R = -r^{-2}\mathcal{G}_{22} + \zeta R = -r^{-2}\left\{rf'(r) + \tfrac{1}{2}r^2 f''(r)\right\} + \zeta R,\\
\mathcal{S}_{33} &= \mathcal{G}^3_3 + \zeta R = -\tfrac{1}{r^2\sin^2\theta}\mathcal{G}_{33} + \zeta R = -r^{-2}\left\{rf'(r) + \tfrac{1}{2}r^2 f''(r)\right\} + \zeta R,
\end{aligned} \tag{5}$$

where the Ricci scalar is given as:

$$R = r^{-2}\{r^2 f''(r) + 4rf'(r) - 2 + 2f(r)\}, \tag{6}$$

where prime notions are the derivative relative to the radial coordinate r. One can elaborate the general total energy-momentum tensor T^μ_i as:

$$T^\mu = E^\mu{}_\nu + \mathcal{T}^\mu_\nu + \theta^\mu_\nu, \tag{7}$$

where $\mathcal{T}^\mu_\nu$ is the energy-momentum tensor for the surrounding field, θ^μ_ν is the energy momentum for quintessence field, and E^μ_ν is the trace-free Maxwell tensor given below as:

$$E_{\mu\nu} = \frac{2}{\kappa}\left(F_{\mu\alpha}F_\nu{}^\alpha - \frac{1}{4}g_{\mu\nu}F^{\alpha\zeta}F_{\alpha\zeta}\right), \tag{8}$$

where $F_{\mu\nu}$ represents the anti-symmetric Faraday tensor, obeying the conditions:

$$\begin{aligned}
F^{\mu\nu}{}_{;\mu} &= 0,\\
\partial_{[\sigma}F_{\mu\nu]} &= 0.
\end{aligned} \tag{9}$$

For spherical symmetry it gives:

$$F^{01} = \frac{Q}{r^2}. \tag{10}$$

Electrostatic charge in this theory is represented by the parameter Q. Hence, the Maxwell tensor takes the form:

$$E^{\mu}{}_{\nu} = \frac{Q^2}{\kappa r^{-4}} \begin{pmatrix} 1 & 0 & 0 & 0 \\ 0 & 1 & 0 & 0 \\ 0 & 0 & -1 & 0 \\ 0 & 0 & 0 & -1 \end{pmatrix}. \tag{11}$$

Letelier was the first to present a solution for a static spherically symmetric black hole in the presence of a cloud of strings [78] in the context of GR. By representing the cloud of strings as world sheets, it is possible to express the energy-momentum tensor of the cloud of strings with a proper density ρ_c given by:

$$\mathcal{T}^{\mu\nu} = \frac{\rho_c \Sigma^{\mu\zeta}\Sigma_{\zeta}{}^{\nu}}{\sqrt{-\gamma}}, \tag{12}$$

where $\gamma = \frac{1}{2}\Sigma^{\mu\nu}\Sigma_{\mu\nu}$. The string bivector $\Sigma^{\mu\nu}$ is expressed as

$$\Sigma^{\mu\nu} = e^{ab}\frac{\partial x^{\mu}}{\partial \xi^{a}}\frac{\partial x^{\nu}}{\partial \xi^{b}}. \tag{13}$$

The two-dimensional Levi-Civita symbol ϵ^{ab}, where $\epsilon^{01} = -\epsilon^{10} = 1$, is utilized here. The spherical symmetry of the cloud of strings is evident, implying that it is solely a function of the radial coordinate r. Consequently, both the density ρ_c and the string bivector $\Sigma^{\mu\nu}$ can be expressed as functions of the radial coordinate r. As a result, the non-zero components of the antisymmetric $\Sigma^{\mu\nu}$ tensor are identified as Σ^{01} and Σ^{10}, and they satisfy the relationship $\Sigma^{01} = -\Sigma^{10}$. Thus, the energy-momentum tensor of the cloud of strings can be written as follows:

$$\mathcal{T}^{\mu}{}_{\nu} = \begin{pmatrix} \rho_c(r) & 0 & 0 & 0 \\ 0 & \rho_c(r) & 0 & 0 \\ 0 & 0 & 0 & 0 \\ 0 & 0 & 0 & 0 \end{pmatrix}. \tag{14}$$

From equations (1), (3) and 14) we may write,

$$\frac{d\rho_c}{dr} + \frac{2\rho_c}{r} = \frac{2\zeta}{4\zeta - 1}\frac{d\rho_c}{dr}. \tag{15}$$

The solution of the above equation reads,

$$\rho_c(r) = br^{-\frac{2(2a-1)}{2(1-1}}, \tag{16}$$

where b is the constant of integration. It has a direct association with the density of the cloud of strings. The weak energy condition stipulates that the value of parameter 'b' must be greater than or equal to zero. Recently, a solution describing a black hole surrounded by quintessence was derived, and its energy-momentum tensor was provided by [79]

$$\theta^{\mu}{}_{\nu} = \begin{pmatrix} \rho_q(r) & 0 & 0 & 0 \\ 0 & \rho_q(r) & 0 & 0 \\ 0 & 0 & -\frac{1}{2}\rho_q(3\omega_q + 1) & 0 \\ 0 & 0 & 0 & -\frac{1}{2}\rho_q(3\omega_q + 1) \end{pmatrix}, \tag{17}$$

where the pressure and density related to quintessence, p_q and ρ_q, respectively, are linked by the equation of state $p_q = \omega_q\rho_q$, with ω_q showing the quintessential state parameter. Now the $\mathcal{S}^0{}_0 = T^0{}_0$ and $\mathcal{S}^1{}_1 = T^1{}_1$ components of Rastall field equations lead [77]:

$$-r^{-2}(rf' - 1 + f) + \frac{\zeta}{r^2}(r^2f'' + 4rf' - 2 + 2f) = \kappa\rho_c + \rho_q(r) + \frac{Q^2}{r^4}. \tag{18}$$

Similarly, the $\mathcal{S}^2_2 = T^2_2$ and $\mathcal{S}^3_3 = T^3_3$ components take the form:

$$-r^{-2}\left(rf' + \frac{1}{2}r^2f''\right) + \frac{\zeta}{r^2}(r^2f'' + 4rf' - 2 + 2f) = -\frac{1}{2}\rho_q(3\omega_q + 1) - \frac{Q^2}{r^4}. \tag{19}$$

Solving equations (17) and (18), we get the general solution for the metric function,

$$f(r) = \left[1 - \frac{2M}{r} + \frac{Q^2}{r^2} + \frac{a(2\zeta - 1)^2 r^{\frac{4\zeta}{1-2\zeta}}}{8\zeta^2 + 2\zeta - 1} - \frac{q}{r^{(3\omega_q+1)}}\right], \tag{20}$$

where $a = \kappa b$. We will define the term a as the cloud of string parameter, as evident from equation (16), where this parameter, or the integration constant b, directly represents the density of the string cloud. The weak energy condition further restricts this parameter, requiring $a \geqslant 0$ [77]. Here, M denotes the mass of the black hole, ω_q

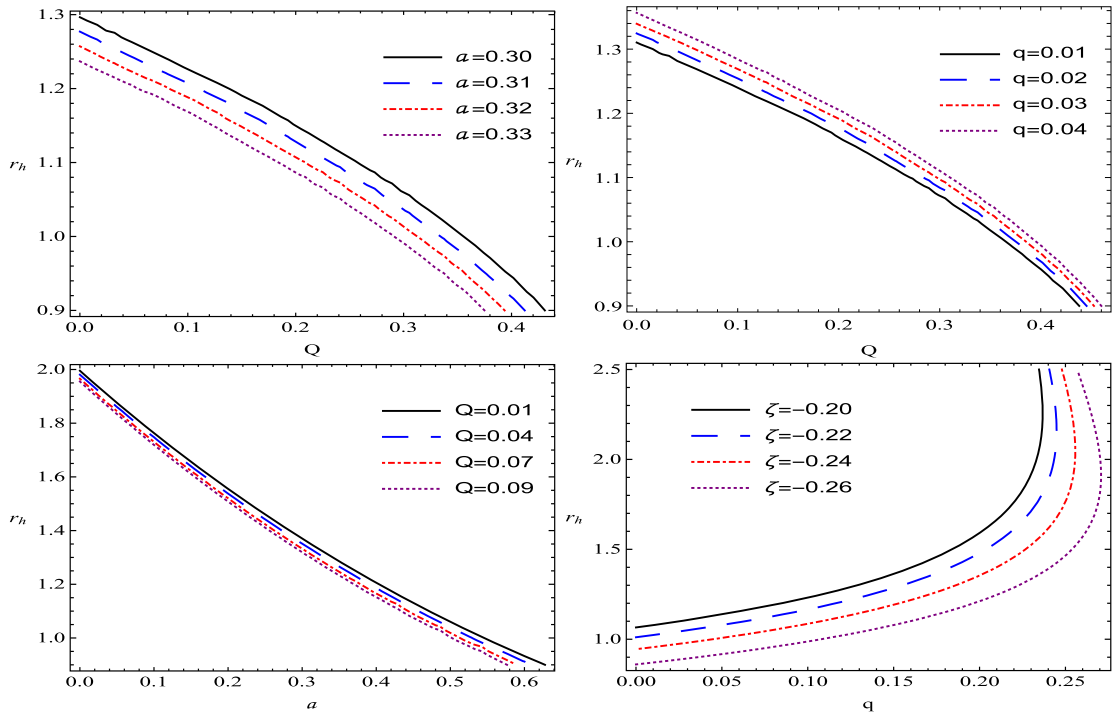

Figure 1. Horizon radius r_h For fixed values $M = 1, q = 0.0001, Q = 0.40$ $a = 0.30$ & $\zeta = -0.20$, where variable values are given in plotlegend.

represents the quintessential state parameter, and q corresponds to the quintessential parameter associated with the quintessence density as defined below. The pressure and density of quintessence are related by the equation of state $p_q = \omega_q \rho_q$, where $\rho_q = -\frac{q}{2}\frac{3\omega_q}{r^{3(\omega_q+1)}}$. To achieve the scenario of accelerated expansion, it is necessary to impose the condition $-1 < \omega_q < -1/3$. In this study, we adopt $\omega_q = -\frac{2}{3}$. As for q, it is a positive parameter [79, 80]. Notably, when $a = q = 0$, we recover the Schwarzschild charged solution.

With equation (20), the metric equation (4) takes the form:

$$ds^2 = \left[1 - \frac{2M}{r} + \frac{Q^2}{r^2} + \frac{a(2\zeta-1)^2 r^{\frac{4\zeta}{1-2\zeta}}}{8\zeta^2 + 2\zeta - 1} - qr\right] dt^2 - \left[1 - \frac{2M}{r} + \frac{Q^2}{r^2} + \frac{a(2\zeta-1)^2 r^{\frac{4\zeta}{1-2\zeta}}}{8\zeta^2 + 2\zeta - 1} - qr\right]^{-1} dr^2 - r^2 d\Omega^2. \tag{21}$$

The metric equation (21) describes a Reissner-Nordström black hole encompassed by a cloud of strings and a quintessence field within the framework of Rastall gravity.

Parameters a, q, Q & ζ have a strong effect on the horizon radius r_h as shown in figure 1. Increasing values of q & ζ result in increasing r_h, while increase in a, Q depict decrease in r_h.

3. Massive particle motion around charged BH surrounded by a cloud of strings and quintessence field (CBHSCSQF) in Rastall gravity

Our analysis begins with the examination of the motion of massive particles around the CBHSCSQF in the context of Rastall gravity. In order to describe the trajectory of such motion, we can employ the Lagrangian of a massive particle with a specified mass M as follows [71]:

$$\mathcal{L}' = \frac{1}{2} g_{\mu\nu} u^\mu u^\nu, \quad u^\mu = \frac{dx^\mu}{d\tau}. \tag{22}$$

In the above equation, τ, x^μ, and u^μ represent the affine parameter, coordinates, and four-velocity of the test particle, respectively. The expressions for the energy $\mathcal{E}$ and angular momentum $\mathcal{L}$, which are crucial quantities governing the dynamics of the test particle, are provided below:

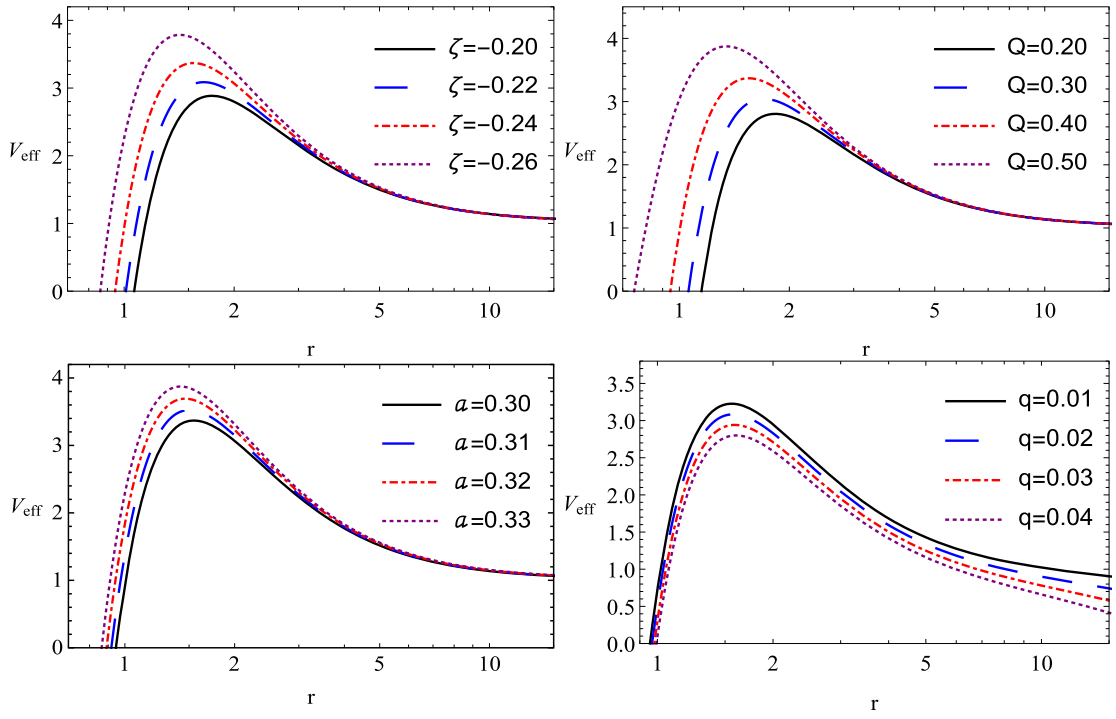

Figure 2. Massive particle: V_{eff} versus r by fixing $\{M=1, q=0.0001, Q=0.40\ \&\ a=0.30$ (Upper eft graph)$\}$, $\{M=1, q=0.0001\ \zeta=-0.20\ \&\ a=0.30$ (Upper right graph)$\}$, $\{M=1, q=0.0001, Q=0.40\ \&\ \zeta=-0.20$ (Lower eft graph)$\}$ and $\{M=1, a=0.3\ \zeta=-0.20\ \&\ Q=0.40$ (Lower right graph)$\}$.

$$\mathcal{E}=\frac{\partial\mathcal{L}'}{\partial u^t}=-f(r)\frac{dT}{d\tau},$$
$$\mathcal{L}=\frac{\partial\mathcal{L}'}{\partial u^\phi}=r^2\sin^2\theta\frac{d\phi}{d\tau}. \tag{23}$$

Equations of motion for test particle can be found by replacing equation (23) into the normalization condition $g_{\mu\nu}u^\mu u^\nu=-\epsilon$ in the equatorial plane $\theta=\frac{\pi}{2}\ \&\ \frac{d\theta}{d\tau}=0$:

$$\frac{dr}{d\tau}=\sqrt{\mathcal{E}^2-f(r)\left(\epsilon+\frac{\mathcal{L}^2}{r^2}\right)}, \tag{24}$$
$$\frac{d\phi}{d\tau}=\frac{\mathcal{L}^2}{r^2\sin^2\theta}, \tag{25}$$
$$\frac{dt}{d\tau}=\frac{\mathcal{E}}{f(r)}, \tag{26}$$

where parameter ϵ is defined in the following condition:

$$\epsilon=\begin{cases}1, & \text{for timelike geodesics}\\ 0, & \text{for null geodesics}\\ -1, & \text{for spacelike geodesics.}\end{cases} \tag{27}$$

Then the equation of geodesics depending upon the radial takes the form:

$$\left(\frac{dr}{d\tau}\right)^2=\mathcal{E}^2-V_{eff}(r)=\mathcal{E}^2-f(r)\left(1+\frac{\mathcal{L}^2}{r^2}\right), \tag{28}$$

where

$$V_{eff}(r)=f(r)\left(1+\frac{\mathcal{L}^2}{r^2}\right). \tag{29}$$

In this case, $V_{eff}(r)$, ϵ, and $\mathcal{L}$ represent the effective potential for the radial motion of the test particle, the geodesic motion, and the angular momentum, respectively. The motion of neutral particles around the black hole can be obtained by imposing the conditions $\dot{r}=0$ and $\ddot{r}=0$. The expressions for $\mathcal{L}^2$ and $\mathcal{E}^2$ for the CBHSCSQF in Rastall gravity are given by:

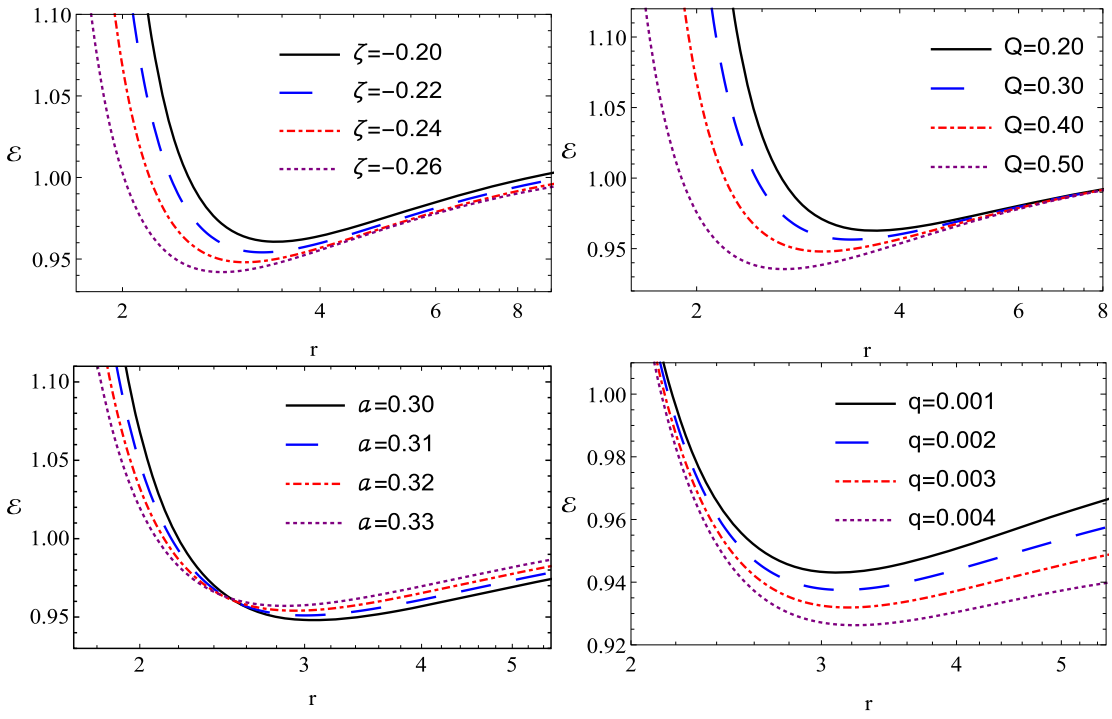

Figure 3. Massive particle: $\mathcal{E}$ versus r by fixing $\{M=1, q=0.0001, Q=0.40\ \&\ a=0.30$ (Upper eft graph)$\}$, $\{M=1, q=0.0001\ \zeta=-0.20\ \&\ a=0.30$ (Upper right graph)$\}$, $\{M=1, q=0.0001, Q=0.40\ \&\ \zeta=-0.20$ (Lower eft graph)$\}$ and $\{M=1, a=0.3\ \zeta=-0.20\ \&\ Q=0.40$ (Lower right graph)$\}$.

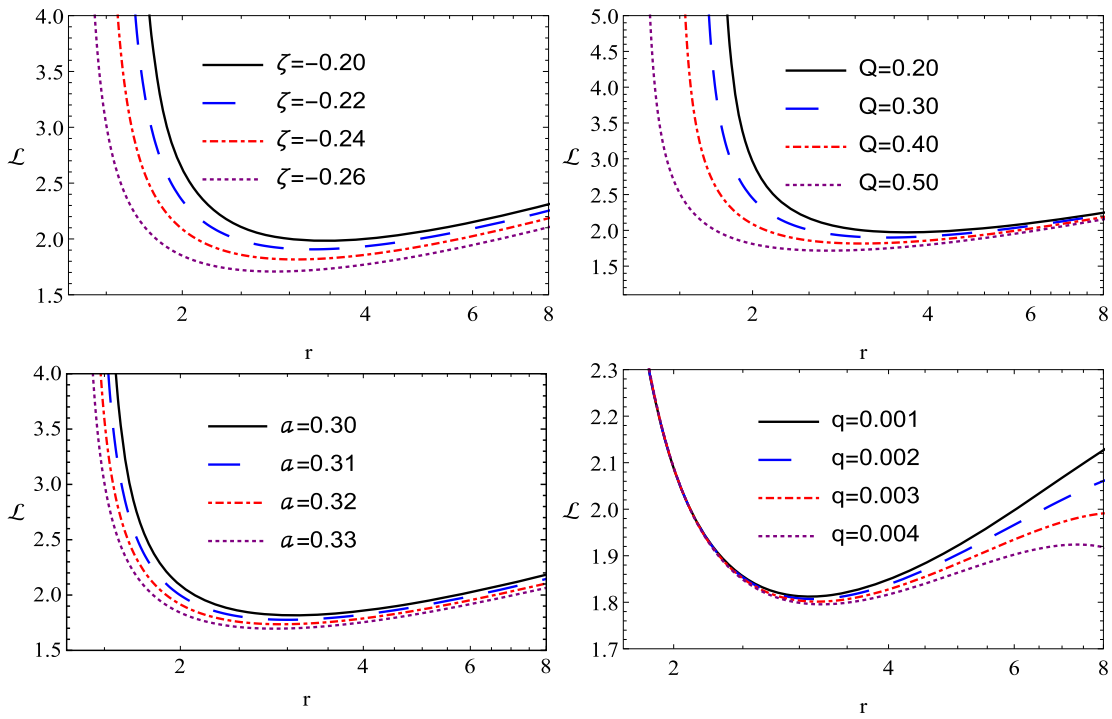

Figure 4. Massive particle: $\mathcal{L}$ versus r by fixing $\{M=1, q=0.0001, Q=0.40\ \&\ a=0.30$ (Upper eft graph)$\}$, $\{M=1, q=0.0001\ \zeta=-0.20\ \&\ a=0.30$ (Upper right graph)$\}$, $\{M=1, q=0.0001, Q=0.40\ \&\ \zeta=-0.20$ (Lower eft graph)$\}$ and $\{M=1, a=0.3\ \zeta=-0.20\ \&\ Q=0.40$ (Lower right graph)$\}$.

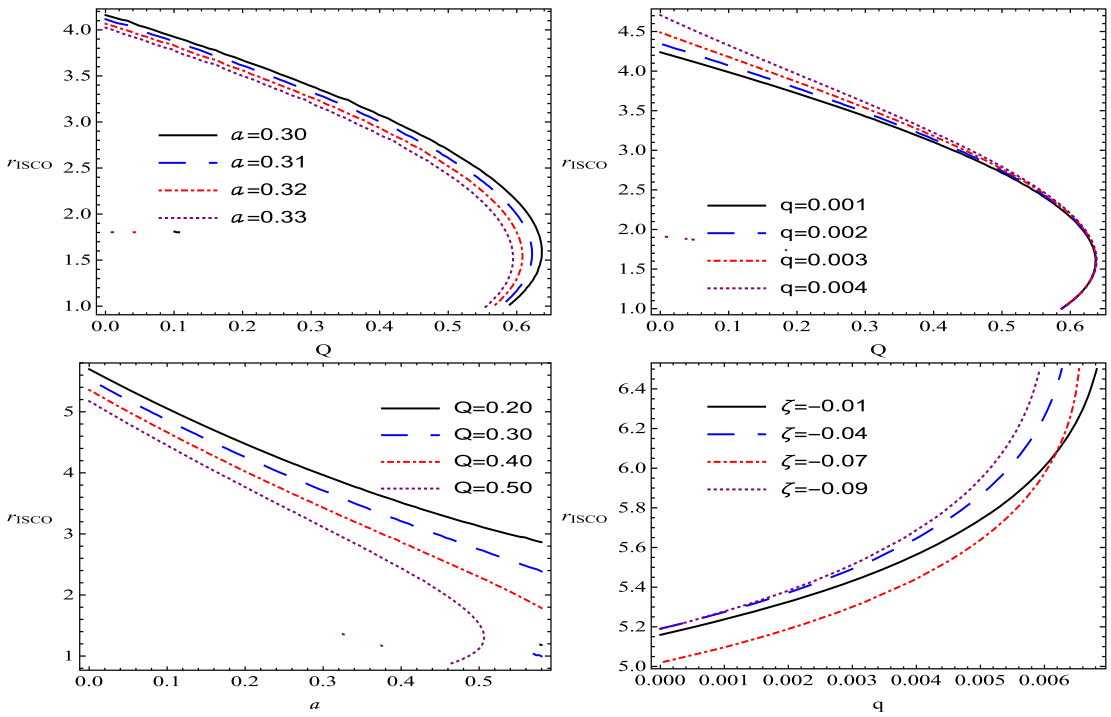

Figure 5. *ISCO* radius r_{ISCO} For fixed values $M = 1, q = 0.0001, Q = 0.40$ $a = 0.30$ & $\zeta = -0.20$, where variable values are given in plotlegend.

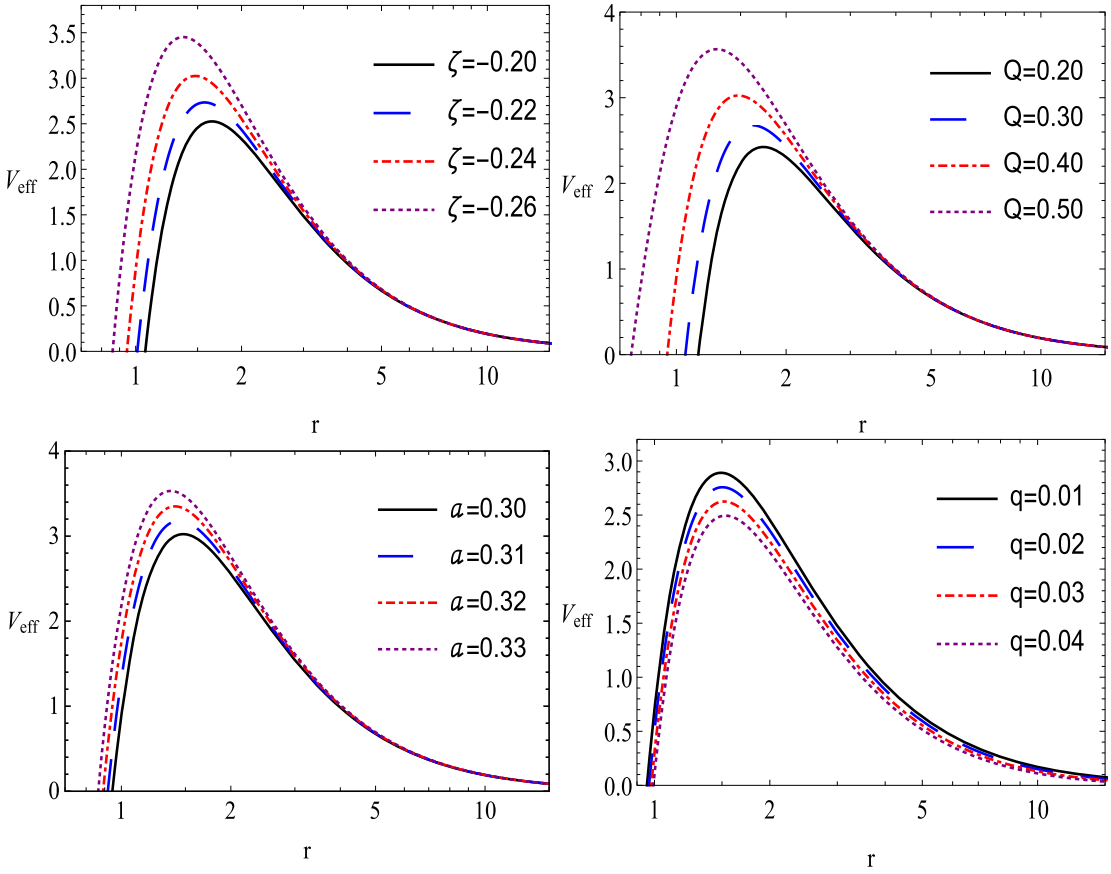

Figure 6. Massless particle: V_{eff} versus r For fixed values $\{M = 1, q = 0.0001, Q = 0.40$ & $a = 0.30$ (Upper eft graph)$\}$, $\{M = 1, q = 0.0001$ $\zeta = -0.20$ & $a = 0.30$ (Upper right graph)$\}$, $\{M = 1, q = 0.0001, Q = 0.40$ & $\zeta = -0.20$ (Lower eft graph)$\}$ and $\{M = 1, a = 0.3$ $\zeta = -0.20$ & $Q = 0.40$ (Lower right graph)$\}$.

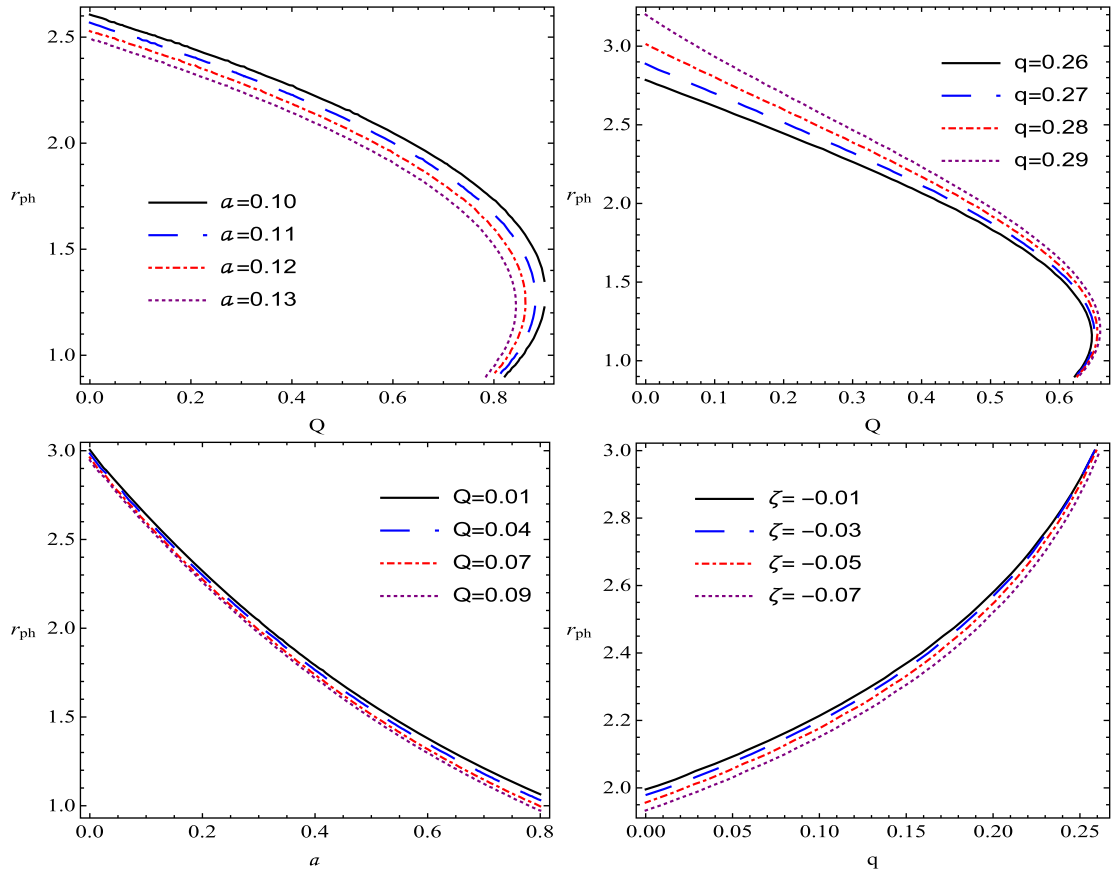

Figure 7. Photon radius r_{Ph} For fixed values $M = 1, q = 0.0001, Q = 0.40$ $a = 0.30$ & $\zeta = -0.20$, where variable values are given in plotlegend.

$$\mathcal{L}^2 = \frac{4a\zeta(2\zeta-1)r^{\frac{2}{1-2\zeta}} + (8\zeta^2+2\zeta-1)r^2\left(-\frac{2(Q-Mr)}{r^2} - qr\right)}{(8\zeta^2+2\zeta-1)\left(\frac{2(r(r-3M)+2Q)}{r^2} - qr\right) - 2a(8\zeta^2-6\zeta+1)r^{\frac{2}{1-2\zeta}-2}}, \tag{30}$$

And

$$\mathcal{E}^2 = \frac{2\left(a(1-2\zeta)^2 r^{\frac{2}{1-2\zeta}-2} + (8\zeta^2+2\zeta-1)\left(qr - \frac{r(r-2M)+Q}{r^2}\right)\right)^2}{(1-4\zeta)^2(2\zeta+1)\left((2\zeta+1)\left(\frac{2(r(r-3M)+2Q)}{r^2} - qr\right) - 2a(2\zeta-1)r^{\frac{2}{1-2\zeta}-2}\right)}. \tag{31}$$

One can observe the radial propagation of V_{eff}, $\mathcal{E}$, and $\mathcal{L}$ in figures 2, 3, and 4, respectively. It is evident that V_{eff} increases with an increase in a & Q, and decreases with an increase in q & ζ. $\mathcal{E}$ shifts towards the left with increasing in a, q, Q and decreasing ζ, Additionally, $\mathcal{L}$ Follows the same trend as $\mathcal{E}$ behaves for varying values of a, Q, q & ζ.

Subsequently, we will investigate the inner stable circular orbit r_{ISCO}. In order to determine the r_{ISCO}, the following conditions can be considered:

$$\begin{cases} V'_{eff} = 0 \\ V''_{eff} = 0. \end{cases} \tag{32}$$

The system complexity makes it difficult to obtain the analytical expression for r_{ISCO}. So, we deal with the *ISCO* radius numerically and draw its graphs depending upon a, Q, q & ζ as shown in figure 5. One can observe by having an overview that r_{ISCO} Decreases with increase in a & Q and increases with increase in q, whereas it shows uneven behavior for decreasing values of ζ.

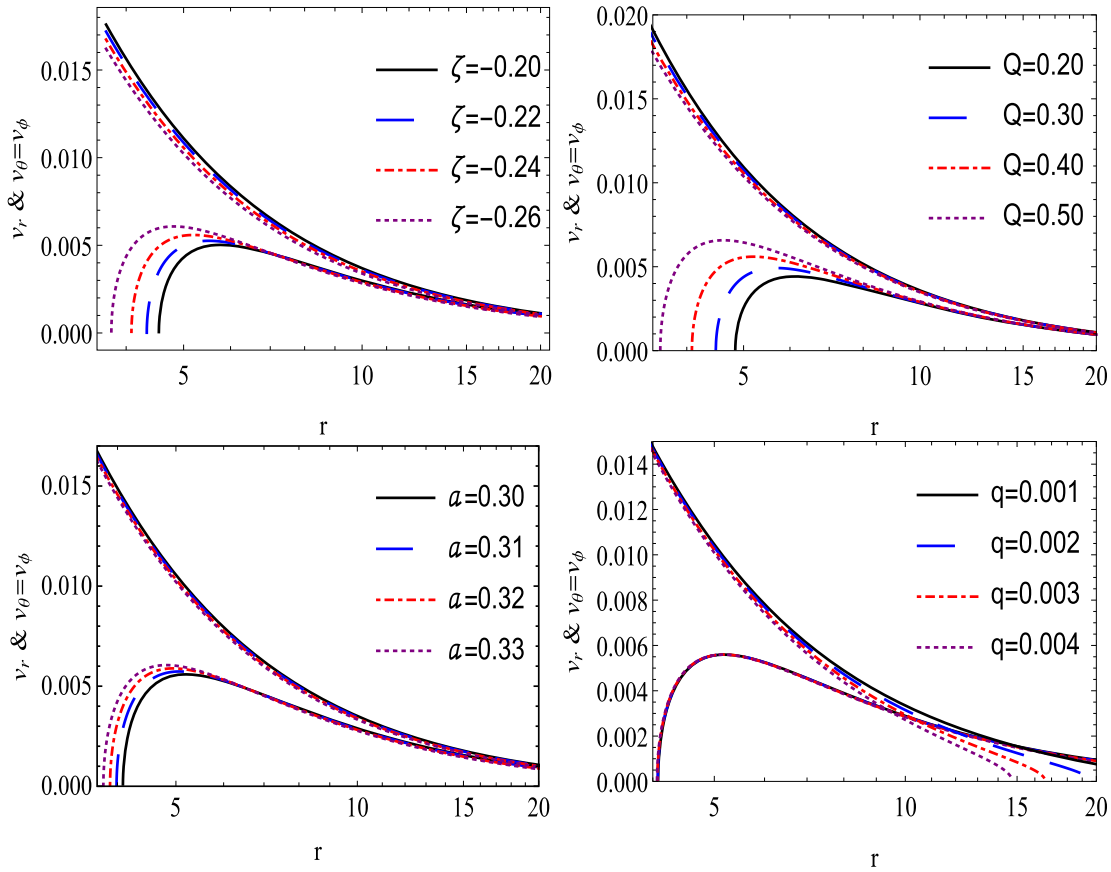

Figure 8. Frequencies v_r & $v_\theta = v_\phi$ verses radial coordinate r by fixing $\{M = 1, q = 0.0001, Q = 0.40$ & $a = 0.30$ (Upper eft graph)$\}$, $\{M = 1, q = 0.0001\ \zeta = -0.20$ & $a = 0.30$ (Upper right graph)$\}$, $\{M = 1, q = 0.0001, Q = 0.40$ & $\zeta = -0.20$ (Lower eft graph)$\}$ and $\{M = 1, a = 0.3\ \zeta = -0.20$ & $Q = 0.40$ (Lower right graph)$\}$.

4. Massless particle otion around BH surrounded by a cloud of strings and quintessence field in Rastall gravity

In this subsection, we investigate the motion of massless particles (photons) within the spacetime of a black hole in Rastall gravity. By employing the metric Lagrangian of the black hole spacetime in Rastall gravity, one can derive the equation of motion for photons around the CBHSCSQF by setting $\epsilon = 0$ in equation (27). In the equatorial plane, the equation of motion can be expressed as:

$$\dot{r}^2 = \mathcal{E}^2 - f(r)\frac{\mathcal{L}^2}{r^2}, \tag{33}$$

$$\dot{\phi} = \frac{\mathcal{L}}{r^2}, \tag{34}$$

$$\dot{t} = \frac{\mathcal{E}}{f(r)}. \tag{35}$$

By Utilizing equation (33), one can easily get the expression for effective potential V_{eff} of the motion of photon as:

$$V_{eff} = f(r)\frac{\mathcal{L}^2}{r^2}. \tag{36}$$

The dependence of the effective potential on the radial coordinate for photon motion is presented in figure 6. The effective potential for massless particles increases with increasing a and Q, while it decreases with increasing q and ζ. The shift in the photon orbit radius can be observed in figure 7. It is observed that the photon radius

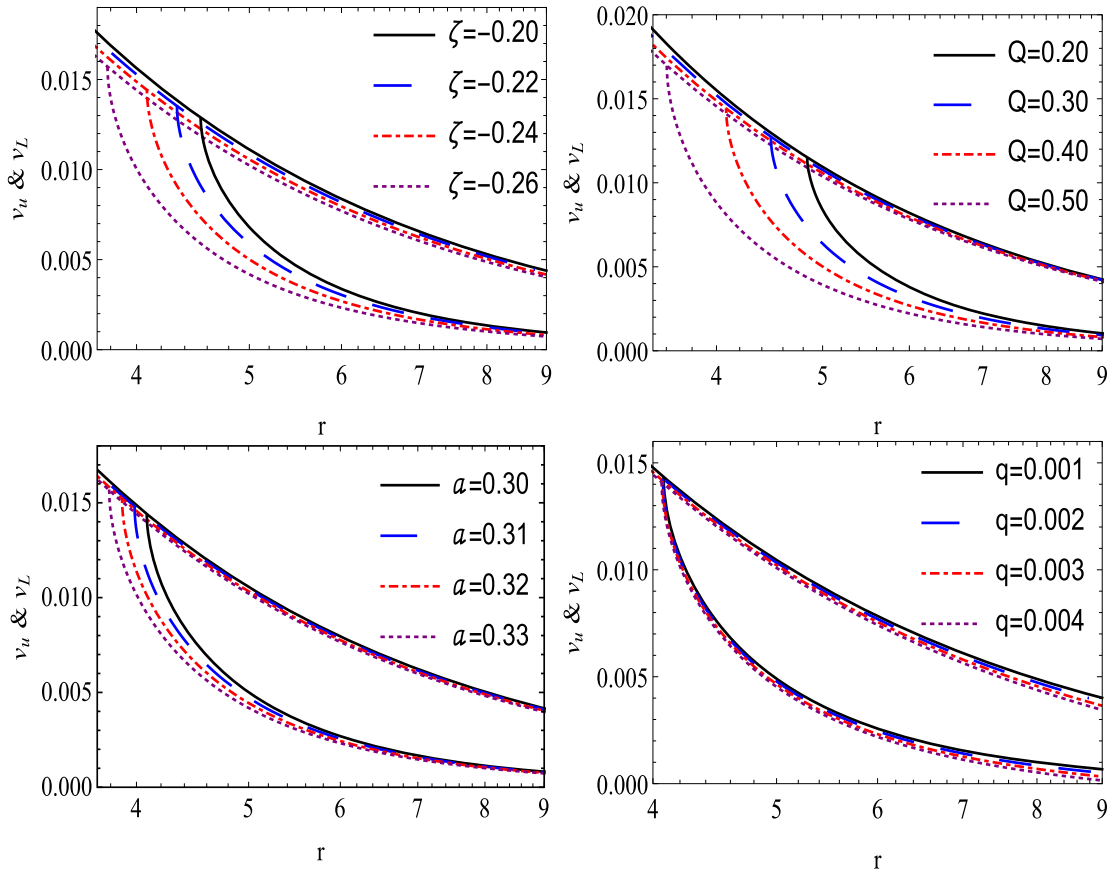

Figure 9. RP-1 Model: Frequencies v_u & v_L verses radial coordinate r by fixing $\{M = 1, q = 0.0001, Q = 0.40$ & $a = 0.30$ (Upper eft graph)$\}$, $\{M = 1, q = 0.0001\ \zeta = -0.20$ & $a = 0.30$ (Upper right graph)$\}$, $\{M = 1, q = 0.0001, Q = 0.40$ & $\zeta = -0.20$ (Lower eft graph)$\}$ and $\{M = 1, a = 0.3\ \zeta = -0.20$ & $Q = 0.40$ (Lower right graph)$\}$.

decreases with an increase in a and Q, and increases with an increase in q and ζ. The photon's circular orbit radius r_{ph} around CBHSCSQF in Rastall gravity can be obtained from the solution of the second equation in equation (32). Being complex solution, we apply numerical method to plot r_{ph} directly without obtaining its expression.

5. Oscillations of massive particles near the circular orbit

In this section, we examine the epicyclic frequencies associated with the quasi-periodic oscillations (QPOs) of test particles within the effective region of the ISCO radius. The detailed formulation of these frequencies can be found in the work by Bambi *et al* [45]. Three fundamental frequencies are considered: (i) the Keplerian frequency or orbital frequency $\nu_\phi = w_\phi/2\pi$, (ii) the radial epicyclic frequency $\nu_r = w_r/2\pi$, which represents the oscillations in the radial direction around the mean orbit, and (iii) the vertical epicyclic frequency $\nu_\theta = w_\theta/2\pi$, which characterizes the vertical oscillations around the mean orbit in time-like equatorial circular orbits. The expressions for these frequencies are given by:

$$w_\phi = \frac{d\phi}{dt} = \frac{-\frac{\partial g_{t\phi}}{\partial r} \pm \sqrt{\left(\frac{\partial g_{t\phi}}{\partial r}\right)^2 - \frac{\partial g_H}{\partial r}\frac{\partial g_{\phi\phi}}{\partial r}}}{\frac{\partial g_{\phi\phi}}{\partial r}}, \tag{37}$$

$$w_r^2 = -\frac{1}{2i^2 g_{rr}}\frac{\partial^2 V_{eff}}{\partial r^2}, \tag{38}$$

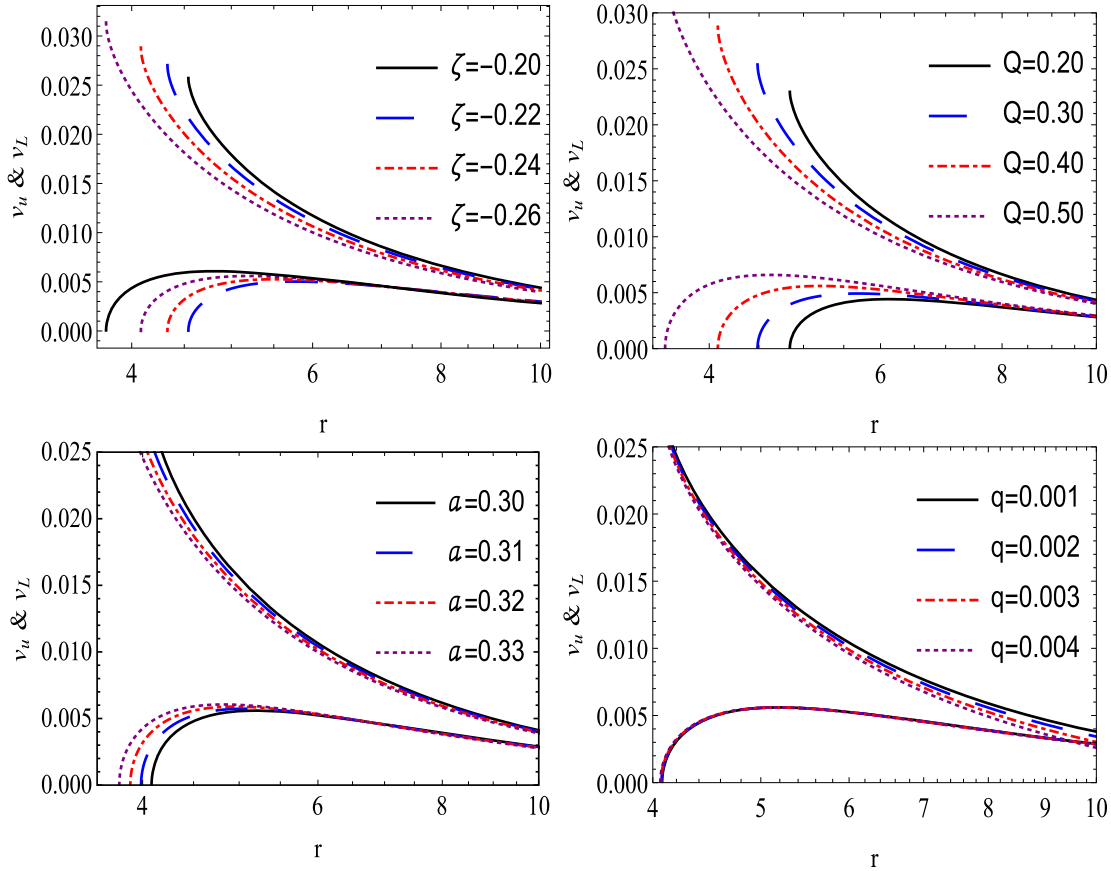

Figure 10. ER-II Model: Frequencies v_u & v_L verses radial coordinate r by fixing $\{M=1, q=0.0001, Q=0.40$ & $a=0.30$ (Upper eft graph)$\}$, $\{M=1, q=0.0001$ $\zeta=-0.20$ & $a=0.30$ (Upper right graph)$\}$, $\{M=1, q=0.0001, Q=0.40$ & $\zeta=-0.20$ (Lower eft graph)$\}$ and $\{M=1, a=0.3$ $\zeta=-0.20$ & $Q=0.40$ (Lower right graph)$\}$.

$$w_\theta^2 = -\frac{1}{2t^2 g_{\theta\theta}}\frac{\partial^2 V_{eff}}{\partial\theta^2}. \tag{39}$$

From the metric space given in equation (20) give the following form of fundamental frequencies of the massive particles around the circular orbits

$$\begin{aligned} v_r = \frac{\sqrt{v_{ar}}}{2\sqrt{2}\,\pi}, \quad \Rightarrow v_{ar} \;=\; & -\frac{2\left(\frac{a(1-2\zeta)^2 r^{\frac{4\zeta}{1-2\zeta}}}{8\zeta^2+2\zeta-1}+\frac{2M}{r}+qr-\frac{Q}{r^2}-1\right)}{(1-2\zeta)^2(-8\zeta^2-2\zeta+1)r^4 v_{1r}^3}[(1-2\zeta)^2 v_{4r} v_{1r}^2[-2a(8\zeta^2-6\zeta+1)r^{\frac{2}{1-2\zeta}} \\ & + 4a\zeta(2\zeta-1)r^{\frac{2}{1-2\zeta}} - (8\zeta^2+2\zeta-1)(-2Mr+qr^3+2Q) + (8\zeta^2+2\zeta-1) \\ & \times(4Q - r(6M + r(qr-2)))] + 2(1-2\zeta)(16\zeta^3-4\zeta^2-4\zeta+1)v_{1r}[4a\zeta(1-2\zeta)r^{\frac{2}{1-2\zeta}} \\ & - 2(8\zeta^2+2\zeta-1)Mr + (8\zeta^2+2\zeta-1)qr^3 + 2(8\zeta^2+2\zeta-1)Q][2(2\zeta+1)Mr \\ & \times(a(2\zeta+1)r^{\frac{2}{1-2\zeta}} + 4(4\zeta-1)qr^3 - 4\zeta Q + Q + (1-4\zeta)r^2) + Q[-4ar^{\frac{2}{1-2\zeta}} \\ & - 9(8\zeta^2+2\zeta-1)qr^3 + 4(8\zeta^2+2\zeta-1)r^2] + 36a\zeta^2 qr^{\frac{2}{1-2\zeta}+3} + aqr^{\frac{2}{1-2\zeta}+3} \\ & - 12a\zeta qr^{\frac{2}{1-2\zeta}+3} - 16a\zeta^2 r^{\frac{2}{1-2\zeta}+2} - 8\zeta^2 qr^5 - 2\zeta qr^5 \;+\; qr^5] - v_{4r}v_{5r}], \end{aligned} \tag{40}$$

$$v_\phi = v_\theta = \frac{\sqrt{\frac{2a\zeta(2\zeta-1)r^{\frac{4\zeta}{1-2\zeta}}}{8\zeta^2+2\zeta-1}+\frac{M}{r}-\frac{qr}{2}-\frac{Q}{r^2}}}{2\pi r}. \tag{41}$$

Where v_{ir}, $i=2, 3\ 4\ldots,14$ are given in Appendix.

These frequencies are contingent upon the spacetime parameters a, q, Q, and ζ, as illustrated in figure 8. It can be observed that v_r increases with increasing values of a, q, and Q, while it decreases with increasing ζ. On the other hand, v_θ decreases with increasing values of a, q, and Q, but increases with increasing ζ.

In this portion of the manuscript, we also account for the possible frequencies of twin peak QPOs [81] surrounded by CBHSCSQF.

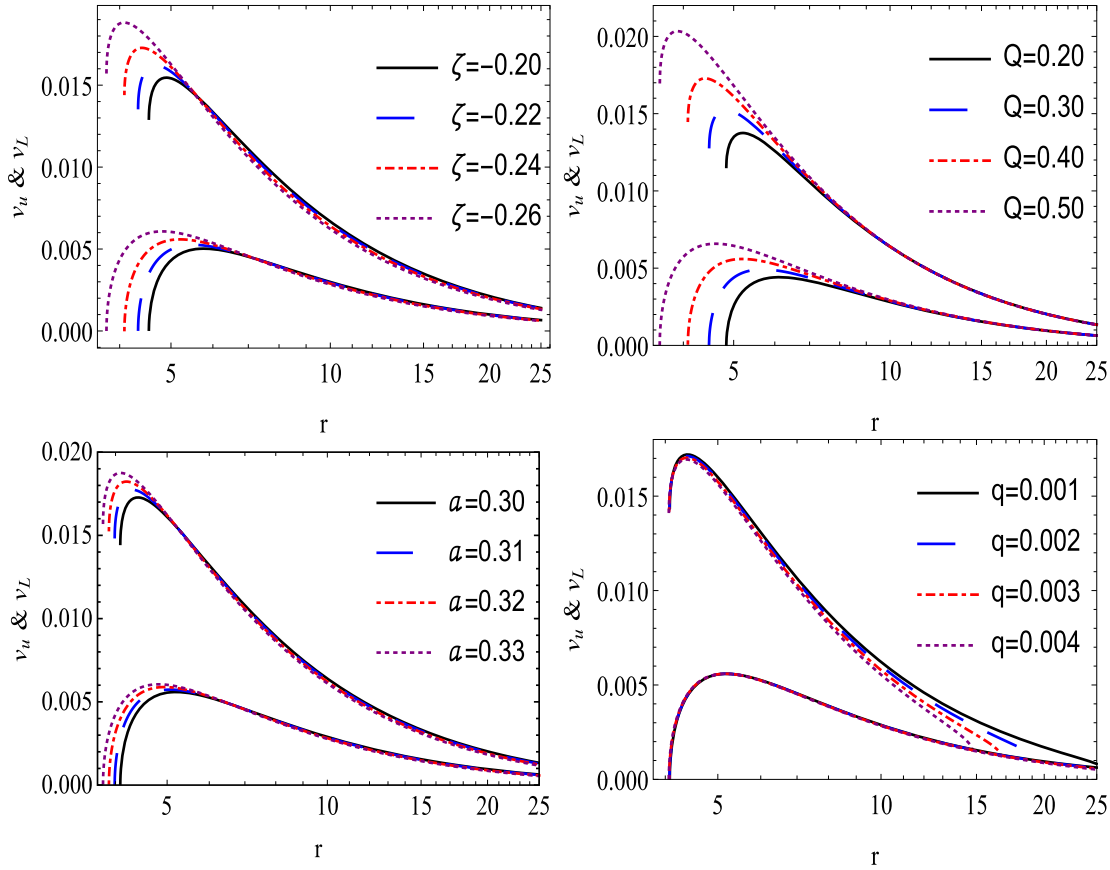

Figure 11. ER-III Model: Frequencies ν_u & ν_L verses radial coordinate r by fixing $\{M = 1, q = 0.0001, Q = 0.40$ & $a = 0.30$ (Upper eft graph)$\}$, $\{M = 1, q = 0.0001\ \zeta = -0.20$ & $a = 0.30$ (Upper right graph)$\}$, $\{M = 1, q = 0.0001, Q = 0.40$ & $\zeta = -0.20$ (Lower eft graph)$\}$ and $\{M = 1, a = 0.3\ \zeta = -0.20$ & $Q = 0.40$ (Lower right graph)$\}$.

- The standard relativistic precession (RP) model [82] assigns upper and lower frequencies based on the respective values of ν_ϕ as $\nu_U = \nu_\phi$ and $\nu_L = \nu_\phi - \nu_r$. In the modified RP-1 model, the frequencies are represented as $\nu_U = \nu_\theta$ and $\nu_L = \nu_\phi - \nu_r$, while in the modified RP-2 model, the frequencies are represented as $\nu_U = \nu_\phi$ and $\nu_L = \nu_\theta - \nu_r$. The graphical representation of the RP model illustrates the increasing and decreasing behaviors associated with changes in the parameters of the CBHSCSQF, as depicted in figure 9.
- The three epicyclic resonance (ER) models, namely ER-II, ER-III, and ER-IV, are proposed in work by Kluzniak *et al* [83]. These models assume that the accretion disks have a significant thickness, and the resonance of radiation particles following geodesic orbits gives rise to quasi-periodic oscillations (QPOs). The upper and lower frequencies for orbital and epicyclic oscillations in the ER models are defined as follows: for the ER-II model, $\nu_U = 2\nu_\theta - \nu_r$ and $\nu_L = \nu_r$ for the ER-III model, $\nu_U = \nu_\theta + \nu_r$ and $\nu_L = \nu_\theta$ and for the ER-IV model, $\nu_U = \nu_\theta + \nu_r$ and $\nu_L = \nu_\theta - \nu_r$. We plot the ER models (ER-II, ER-III, ER-IV) incorporating the effects of CBHSCSQF geometry parameters in figures 10, 11, and 12).

6. Effective force

The determination of the movement of a test particle, whether it is directed away or towards the central source, can be inferred by observing the behavior of the effective force. The effective force experienced by a test particle within the gravitational field of a gravitating source [84] can be calculated using the following expression:

$$F = -\frac{1}{2}\frac{\partial\ V_{eff}(r)}{\partial r}. \tag{42}$$

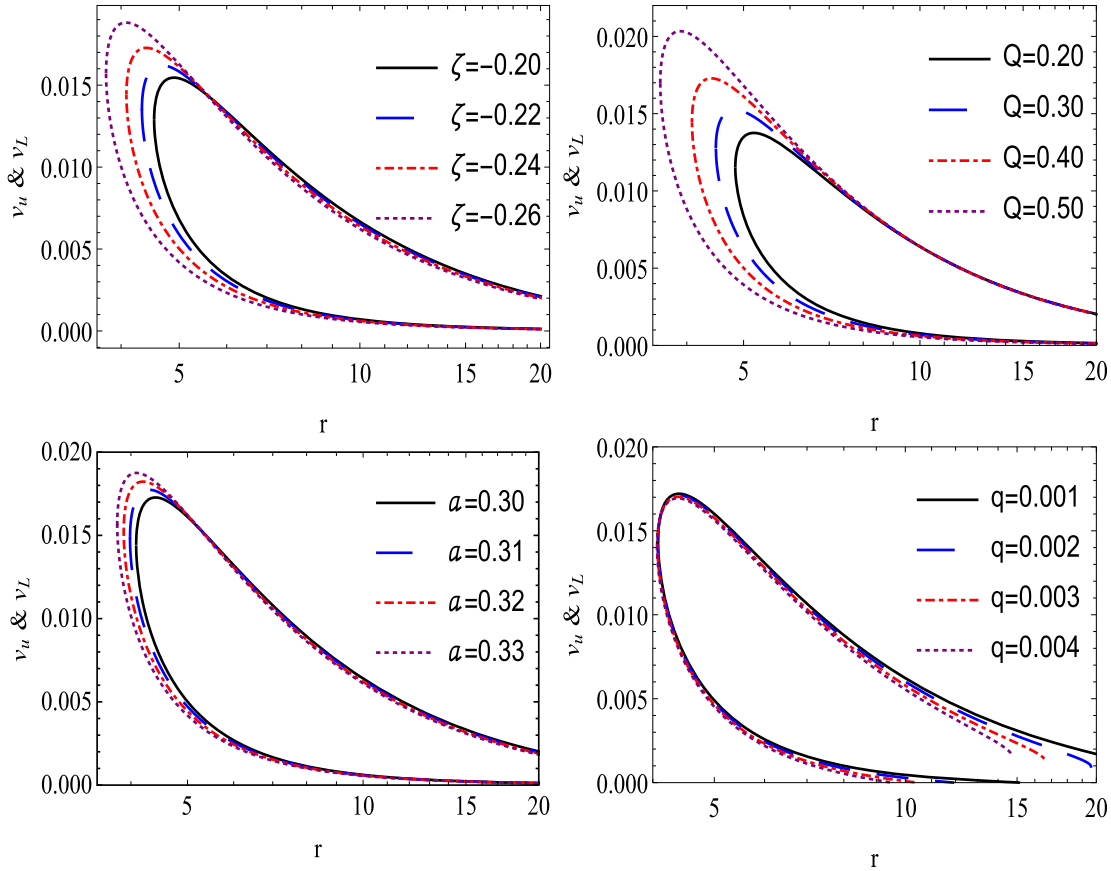

Figure 12. ER-IV Model: Frequencies ν_u & ν_L verses radial coordinate r by fixing $\{M=1, q=0.0001, Q=0.40$ & $a=0.30$ (Upper eft graph)$\}$, $\{M=1, q=0.0001\ \zeta=-0.20$ & $a=0.30$ (Upper right graph)$\}$, $\{M=1, q=0.0001, Q=0.40$ & $\zeta=-0.20$ (Lower eft graph)$\}$ and $\{M=1, a=0.3\ \zeta=-0.20$ & $Q=0.40$ (Lower right graph)$\}$.

The expression of effective force calculated in the case of CBHSCSQF in Rastall gravity geometry is as:

$$
\begin{aligned}
F \;=\; & -\frac{1}{2r^3}\left[\left[\frac{4a\zeta(2\zeta-1)r^{\frac{2}{1-2\zeta}}}{8\zeta^2+2\zeta-1}+2Mr-qr^3-2Q\right]\right.\\
& \times\left[\frac{4a\zeta(2\zeta-1)r^{\frac{2}{1-2\zeta}}-(8\zeta^2+2\zeta-1)(-2Mr+qr^3+2Q)}{r^2\left((8\zeta^2+2\zeta-1)\left(-\frac{6M}{r}-qr+\frac{4Q}{r^2}+2\right)-2a(8\zeta^2-6\zeta+1)r^{\frac{4\zeta}{1-2\zeta}}\right)}+1\right]\\
& +\frac{2}{(1-4\zeta)^2\left(-2ar^{\frac{4\zeta}{1-2\zeta}}+4a\zeta r^{\frac{4\zeta}{1-2\zeta}}-4\zeta+\frac{6(2\zeta+1)M}{r}+2\zeta qr\;+\;qr-\frac{4(2\zeta+1)Q}{r^2}-2\right)^2}[[4a\zeta^2r^{\frac{4\zeta}{1-2\zeta}}\\
& +ar^{\frac{4\zeta}{1-2\zeta}}-4a\zeta r^{\frac{4\zeta}{1-2\zeta}}-8\zeta^2-2\zeta+\frac{2(8\zeta^2+2\zeta-1)M}{r}+(8\zeta^2+2\zeta-1)qr\\
& \left.+\frac{(-8\zeta^2-2\zeta+1)Q}{r^2}+1\right]\\
& \times\left[-\frac{2(2\zeta+1)M(a(2\zeta+1)r^{\frac{2}{1-2\zeta}}+4(4\zeta-1)qr^3-4\zeta Q+Q+(1-4\zeta)r^2)}{r}-a(1-6\zeta)^2qr^{\frac{2}{1-2\zeta}+1}\right.\\
& \left.+4Q(ar^{\frac{4\zeta}{1-2\zeta}}-8\zeta^2-2\zeta+1)+16a\zeta^2r^{\frac{2}{1-2\zeta}}+9(8\zeta^2+2\zeta-1)qQr+(8\zeta^2+2\zeta-1)qr^3]]\right].
\end{aligned}
\tag{43}
$$

The interpretation of the impact of the effective force can be enhanced through graphical analysis, as depicted in figure 13. It is observed that the behavior of the effective force fluctuates between attractive and repulsive, eventually settling into an attractive force along the radial motion. The attractiveness of the effective force increases with an increase in q and becomes more repulsive with an increase in Q. On the other hand, when a is

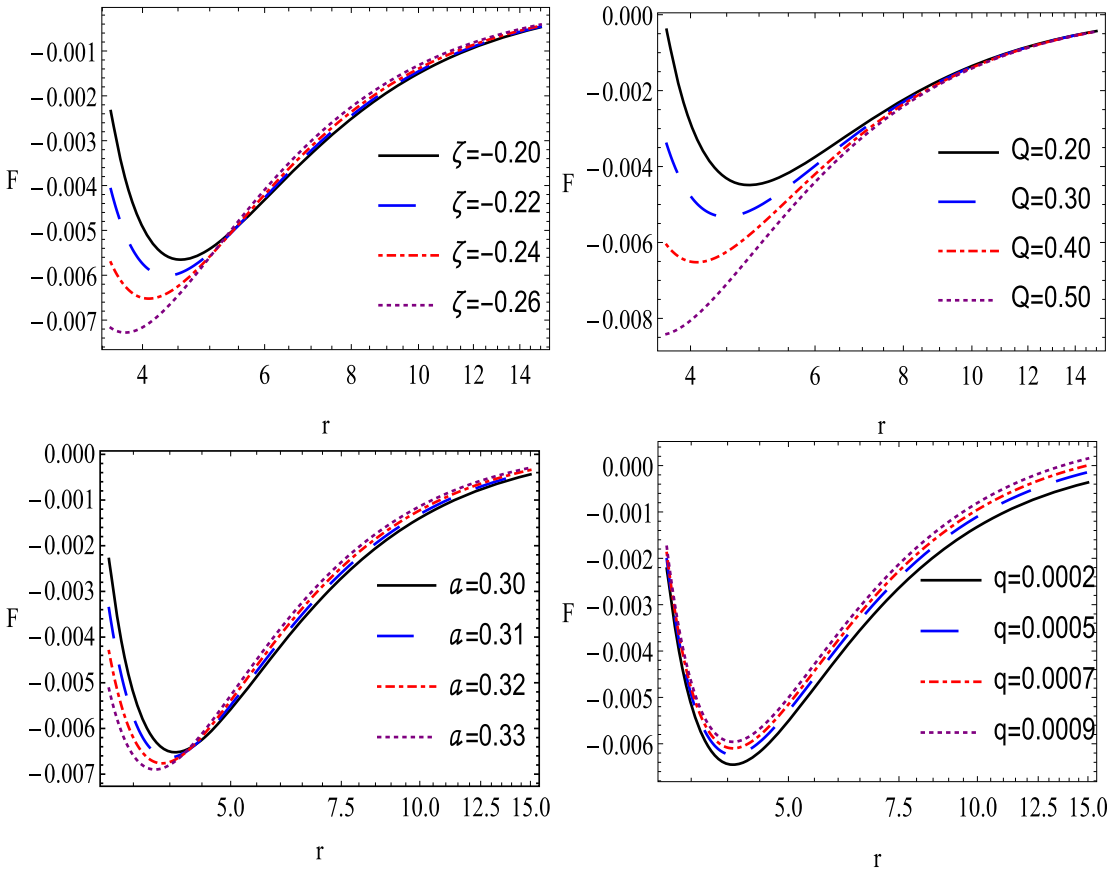

Figure 13. Effective Force F verses radial coordinate r by fixing $\{M=1, q=0.0001, Q=0.40\ \&\ a=0.30$ (Upper eft graph)$\}$, $\{M=1, q=0.0001\ \zeta=-0.20\ \&\ a=0.30$ (Upper right graph)$\}$, $\{M=1, q=0.0001, Q=0.40\ \&\ \zeta=-0.20$ (Lower eft graph)$\}$ and $\{M=1, a=0.3\ \zeta=-0.20\ \&\ Q=0.40$ (Lower right graph)$\}$.

increased, the effective force is initially attractive but later becomes repulsive. Similarly, decreasing ζ leads to an initial repulsive effective force, followed by it becoming attractive.

7. Conclusion and summary

This paper contains a comprehensive discussion of the particle motion for massive and massless particles, quasi-periodic oscillations, and effective force under the paradigm of Rastall gravity with charge of black hole, strings of cloud, and quintessence field. Through the above discussion, we reached the following concluding points:

- We Plotted the horizon radius r_h in figure 1 along parameters Q, a & q. It can obviously be seen that the horizon radius r_h along Q increases with the increasing q and decreases with increasing a. Horizon radius r_h along a decreases with the increasing Q, and horizon radius r_h along q increases with the increasing ζ.
- While studying the particle dynamics around the Rastall BH, we discussed the effective potential V_{eff} depending upon the radial coordinate r of the compact body for massive and massless particles for varying values of ζ, Q, a & q. It can be observed from figure 2 for massive particles and figure 6 for massless particles that the V_{eff} increases by increasing Q & a and decreases by increasing ζ & q. Moreover, V_{eff} for the massive particle is more than the massless particle.
- One can observe the energy and angular momentum of massive particles in figures 3 and 4. Energy and angular momentum along radial coordinate r, increase with the increase in ζ and decrease with an increase in Q, q & a.
- We investigate the ISCO radius for massive particles around the BH, it is observable from figure 5 that ISCO along Q increases with an increase in q and decreases with the increasing values of a. Moreover ISCO along a increases with an increase in Q, and along q increases with the increase in ζ.

- Photon sphere radius is investigated, studied, and calculated by using the common method using the effective potential. Its detailed information can be seen in figure 7. r_{ph} along Q increases with an increase in q and decreases with the increasing values of a. Also, r_{ph} along a decreases with an increase in Q, and along q increases with the increase in ζ.
- We plotted the radial and tangential frequencies along radial coordinate r in figure 8. In figure 9, we plot the upper and lower frequencies of the RP model while ER model frequencies are given in figures 10, 11, and 12. These graphical illustrations indicate variations in the frequencies by varying the parameters Q q a & ζ (Q is electrostatic charge, q is a positive parameter, a is cloud of string parameter, and ζ is Rastall parameter).
- Attractive behavior of the test particle through the effective force is plotted in figure 13 along the BH radius r in Rastall gravity under the effects of Rastall parameter ζ, the quintessential parameter q, charge Q, and string parameter a.
- Significantly, we obtained the outcomes within the context of the quintessence field and charged strings of cloud. The computed findings we present are authentic and grounded in theoretical prognostications, thus holding the potential for facilitating forthcoming investigations.

Acknowledgments

The work was supported in part by NSFC under grants 12 271 488, 11 975 145 and 11 972 291, the Ministry of Science and Technology of China (G2021016032L), and the Natural Science Foundation for Colleges and Universities in Jiangsu Province (17 KJB 110 020). Asif Mahmood would like to acknowledge the Researcher's Supporting Project Number (RSP2024R43), King Saud University, Riyadh, Saudi Arabia.

Data availability statement

There is no data. Only calculations can be shared. The data that support the findings of this study are available upon reasonable request from the authors.

Appendix

$$
\begin{aligned}
v_{1r} &= (8\zeta^2 + 2\zeta - 1)(4Q - r(6M + r(qr - 2))) - 2a(8\zeta^2 - 6\zeta + 1)r^{\frac{2}{1-2\zeta}},\\
v_{2r} &= 4a\zeta(2\zeta - 1)r^{\frac{2}{1-2\zeta}} - (8\zeta^2 + 2\zeta - 1)(-2Mr + qr^3 + 2Q),\\
v_{3r} &= -8a\zeta r^{\frac{2}{1-2\zeta}} - 6M(2\zeta r + r) + 2\zeta qr^3 + qr^3 + 8(2\zeta + 1)Q,\\
v_{4r} &= a(1 - 2\zeta)^2 r^{\frac{2}{1-2\zeta}} + 2(8\zeta^2 + 2\zeta - 1)Mr + (8\zeta^2 + 2\zeta - 1)qr^3\\
&\quad + (-8\zeta^2 - 2\zeta + 1)Q + (-8\zeta^2 - 2\zeta + 1)r^2,\\
v_{5r} &= (2\zeta - 1)(2\zeta + 1)(-(1 - 4\zeta)^2)(3(8\zeta^2 - 6\zeta + 1)qr^3 - 4a\zeta r^{\frac{2}{1-2\zeta}})[-2ar^{\frac{2}{1-2\zeta}} + 4a\zeta r^{\frac{2}{1-2\zeta}}\\
&\quad + 6M(2\zeta r + r) + 2\zeta qr^3 + qr^3 - 4(2\zeta + 1)Q - 4\zeta r^2 - 2r^2]^2 \quad + \quad 2(1 - 2\zeta)^2 v_{1r}^2\\
&\quad \times (8a\zeta r^{\frac{2}{1-2\zeta}} - 2(8\zeta^2 + 2\zeta - 1)Mr \quad + \quad 3(8\zeta^2 + 2\zeta - 1)qr^3) + (1 - 2\zeta)(8\zeta^2 - 6\zeta + 1)v_{1r}v_{3r}\\
&\quad \times (8a\zeta r^{\frac{2}{1-2\zeta}} - 2(8\zeta^2 + 2\zeta - 1)Mr \quad + \quad 3(8\zeta^2 + 2\zeta - 1)qr^3) + 2(8\zeta^2 - 6\zeta + 1)v_{1r}v_{2r}\\
&\quad \times (2a\zeta(6\zeta - 1)r^{\frac{2}{1-2\zeta}} + 3(4\zeta^2 - 1)Mr + (6 - 24\zeta^2)Q) + (8\zeta^2 - 6\zeta + 1)^2 v_{2r}v_{3r}^2 \quad + \quad 2(1 - 2\zeta)\\
&\quad \times (8\zeta^2 - 6\zeta + 1)v_{1r}v_{2r}v_{3r} + 3(1 - 2\zeta)^2 v_{1r}^2 v_{2r}
\end{aligned}
$$

ORCID iDs

Asifa Ashraf https://orcid.org/0000-0001-5522-5491
Allah Ditta https://orcid.org/0000-0001-7758-8736
Değer Sofuoğlu https://orcid.org/0000-0002-8842-7302
Wen-Xiu Ma https://orcid.org/0000-0001-5309-1493
Faisal Javed https://orcid.org/0000-0001-6970-1305
Farruh Atamurotov https://orcid.org/0000-0001-8857-4970
Asif Mahmood https://orcid.org/0000-0003-1803-8384

References

[1] Will C M and Relativ L R 2014 *Living Rev. Relativ.* **17** 4
[2] Hulse R A and Taylor J H 1975 *ApJL* **195** L51
[3] Damour T and Taylor J H 1992 *Phys. Rev.* D **45** 1840
[4] Abbott B P *et al* 2016 *Phys. Rev. Lett.* **116** 061102
[5] Abbott B P *et al* 2016 *Phys. Rev. Lett.* **116** 241103
[6] Abbott B P *et al* 2016 *Phys. Rev.* D **93** 122008
[7] Abbott B P *et al* 2017 *Phys. Rev.* D **96** 122006
[8] Abbott B P *et al* 2017 *Phys. Rev. Lett.* **119** 161101
[9] Burns E *et al* 2019 *ApJ* **87** 1
[10] Abbott B P *et al* 2020 *Phys. Rev.* D **102** 043015
[11] Abbott R *et al* 2021 *ApJL* **915** L5
[12] Riess A G *et al* 1998 *Astron. J* **116** 1009
[13] Perlmutter S *et al* 1999 *ApJ* **517** 565
[14] Stelle K S 1977 *Phys. Rev.* D **16** 953
[15] Bahcall N A 1999 *Science* **284** 1481
[16] Perez de los Heros C 2020 *Symmetry* **12** 1648
[17] Bull P *et al* 2016 *Phys. Dark Universe* **12** 56
[18] Amendola L and Tsujikawa S 2010 *Dark Energy: Theory and Observations* (Cambridge University Press)
[19] Gogoi D J and Dev Goswami U 2022 *Indian J. Phys.* **96** 637–46
[20] Miller M C and Yunes N 2019 *Nature* **568** 469
[21] Gogoi D J and Goswami U D 2021 *Phys. Dark Universe* **33** 100860
[22] Ezquiaga J M and Zumalacárregui M 2018 *Front. Astron. Space Sci.* **5** 44
[23] Abbott B P *et al* 2017 *Phys. Rev. Lett.* **118** 221101
[24] Rastall P 1972 *Phys. Rev. D* **6** 3357
[25] De Moraes W A G and Santos A F 2019 *Gen. Relativ. Gravit.* **51** 167
[26] Shabani H and Hadi Ziaie A 2020 *EPL* **129** 20004
[27] Darabi F, Moradpour H, Licata I, Heydarzade Y and Corda C 2018 *Eur. Phys. J. C* **78** 25
[28] Heydarzade Y and Darabi F 2017 *Phys. Lett.* B **771** 365
[29] Heydarzade Y, Moradpour H and Darabi F 2017 *Can. J. Phys.* **95** 1253
[30] Kumar R and Ghosh S G 2018 *Eur. Phys. J. C* **78** 750
[31] Ziaie A H, Moradpour H and Ghaffari S 2019 *Phys. Lett. B* **793** 276
[32] Batista C E M, Daouda M H, Fabris J C, Piattella O F and Rodrigues D C 2012 *Phys. Rev. D* **85** 084008
[33] Javed F *et al* 2022 *Eur. Phys. J. Plus* **61** 137
Javed F *et al* 2022 *Fortschr. Phys* **2022** 2200053
Javed F *et al* 2022 *Euro. Phys. J. C* **82** 825
Javed F *et al* 2022 *Phys. Scr.* **97** 125010
Javed F *et al* 2023 *Fortschr. Phys* **2023** 2200214
Javed F *et al* 2023 *Nucl. Phys. B* **990** 116180
[34] Visser M 2018 *Phys. Lett. B* **782** 83
[35] Darabi F, Atazadeh K and Heydarzade Y 2018 *Eur. Phys. J. Plus* **133** 249
[36] Darabi F, Moradpour H, Licata I, Heydarzade Y and Corda C 2018 *Eur. Phys. J. C* **78** 1
[37] Hansraj S, Banerjee A and Channuie P 2019 *Ann. Phys.* **400** 320
[38] Ditta A, Tiecheng X, Mustafa G and Errehymy A 2023 *Eur. Phys. J. C* **83** 1020
[39] Ditta A and Tiecheng X 2022 *Chin. J. Phys.* **79** 57–68
[40] Ditta A, Xia T, Mahmood I and Mahmood A 2024 *Chin. Phys. B* **33** 030204
[41] Bambi C 2012 *Phys. Rev. D* **85** 043002 arXiv:1201.1638 [gr-qc]
[42] Bambi C, Jiang J and Steiner J F 2016 *Class. Quantum Grav.* **33** 064001
[43] Zhou M, Cao Z, Abdikamalov A, Ayzenberg D, Bambi C, Modesto L and Nampalliwar S 2018 *Phys. Rev. D* **98** 024007
[44] Tripathi A *et al* 2019 arXiv:1901.03064 [gr-qc]
[45] Bambi C 2017 *Black Holes: A Laboratory for Testing Strong Gravity* (Springer)
[46] Chandrasekhar S 1998 *The mathematical theory of black holes* (Oxford University Press)
[47] Chen S, Wang M and Jing J 2016 *J. High Energy Phys.* **2016** 82
[48] Hashimoto K and Tanahashi N 2017 *Phys. Rev. D* **95** 024007
[49] Dalui S, Majhi B R and Mishra P 1803 *Phys. Lett. B* **788** 486
[50] Han W 2008 *Gen. Relativ. Gravit.* **40** 1831–47
[51] Morozova V S, Rezzolla L and Ahmedov B J 2014 *Phys. Rev. D* **89** 104030
[52] Jamil M, Hussain S and Majeed B 2015 *Eur. Phys. J. C* **75** 24
[53] Hussain S, Hussain I and Jamil M 2014 *Eur. Phys. J. C* **74** 210
[54] Bañados M, Silk J and West S M 2009 *Phys. Rev. Lett.* **103** 111102
[55] Shaymatov S R, Ahmedov B J and Abdujabbarov A A 2013 *Phys. Rev. D* **88** 024016
[56] Narzilloev B, Malafarina D, Abdujabbarov A and Bambi C 2020 *Eur. Phys. J. C* **80** 784
[57] Narzilloev B, Rayimbaev J, Abdujabbarov A and Bambi C 2005 *Eur. Phys. J. C* **80** 1074
[58] Narzilloev B, Rayimbaev J, Shaymatov S, Abdujabbarov A, Ahmedov B and Bambi C 2020 *Phys. Rev. D* **102** 044013
[59] Narzilloev B, Rayimbaev J, Shaymatov S, Abdujabbarov A, Ahmedov B and Bambi C 2011 *Phys. Rev. D* **102** 104062
[60] Narzilloev B, Rayimbaev J, Abdujabbarov A, Ahmedov B and Bambi C 2021 *Eur. Phys. J. C* **81** 269
[61] Abdujabbarov A, Ahmedov B, Rahimov O and Salikhbaev U 2014 *Phys. Scr.* **89** 084008
[62] Rahimov O G, Abdujabbarov A A and Ahmedov B J 2011 *Astrophys. Space Sci.* **335** 499
[63] Rahimov O G 2011 *Mod. Phys. Lett. A* **26** 399
[64] Haydarov K, Abdujabbarov A, Rayimbaev J and Ahmedov B 2020 *Universe* **6** 44
[65] Rayimbaev J, Figueroa M, Stuchlík Z and Juraev B 2020 *Phys. Rev. D* **101** 104045
[66] Turimov B, Rayimbaev J, Abdujabbarov A, Ahmedov B and Stuchlík Z c v 2020 *Phys. Rev. D* **102** 064052

[67] Ditta A, Xia T and Yasir M 2023 *Int. J. Mod. Phys. A* **38** 2350041
[68] Ditta A, Xia T, Mumtaz S, Atamurotov F, Mustafa G and Abdujabbarov A 2023 *Phys. Dark Universe* **41** 101248
[69] Ditta A, Xia T, Atamurotov F, Mustafa G and Aripov M M 2023 *Chin. J. Phys.* **83** 664–79
[70] Atamurotov F, Ortiqboev D, Abdujabbarov A and Mustafa G 2022 *Eur. Phys. J. C* **82** 659
[71] Atamurotov F, Alloqulov M, A Abdujabbarov and Ahmedov B 2022 *Eur. Phys. J. Plus* **137** 634
[72] Atamurotov F, Shaymatov S, Sheoran P and Siwach S 2021 *J. Cosmol. Astropart. Phys.* **2021** 045
[73] Babar G Z, Atamurotov F, Islam S U and Ghosh S G 2021 *Phys. Rev. D* **103** 084057
[74] Mustafa G, Atamurotov F, Hussain I, Shaymatov S and Ovgun A 2022 *Chin. Phys. C* **46** 125107
[75] Atamurotov F, Hussain I, Mustafa G and Ovgun A 2023 *Chin. Phys. C* **47** 025102
[76] Atamurotov F, Hussain I, Mustafa G and Jusufi K 2022 *Eur. Phys. J. C* **82** 831
[77] Jyoti Gogoi D, Karmakar R and Goswami U D 2021 arXiv:2111.00854
[78] Letelier P S 1979 *Phys. Rev. D* **20** 1294
[79] Kiselev V V 2003 *Class. Quantum Grav.* **20** 1187
[80] Toledo J d and Bezerra V B 2018 *Eur. Phys. J. C* **78** 534
[81] Rayimbaev J, Shaymatov S and Jamil M 2021 *Eur. Phys. J. C* **81** 699
[82] Stella L, Vietri M and Morsink S M 1999 *Astrophys. J.* **524** L63
[83] Abramowicz M A and Kluzniak W 2001 *Astron. Astrophys.* **374** L19
[84] Fernando S 2012 *Gen. Relativ. Gravit.* **44** 1857